Purine Nucleoside Phosphorylase. 1. Structure−Function Studies†

Mark D. Erion,*,‡ Kenji Takabayashi,‡ Harry B. Smith,‡ Janine Kessi,‡ Sylvia Wagner,‡ Sybille Hönger,‡ Spencer L. Shames,§ and Steven E. Ealick||

Central Research Laboratory, Ciba-Geigy Ltd., Basel, Switzerland CH4002, Research Department, Pharmaceuticals Division, Ciba-Geigy Corp., Summit, New Jersey 07901, and Department of Biochemistry, Molecular and Cell Biology, Cornell University, Ithaca, New York, 14853

Received August 7, 1996; Revised Manuscript Received June 30, 1997⊗

ABSTRACT: To probe the catalytic mechanism of human purine nucleoside phosphorylase (PNP), 13 active-site mutants were constructed and characterized by steady-state kinetics. In addition, microtiter plate assays were developed for both the phosphorolytic and synthetic reactions and used to determine the kinetic parameters of each mutant. Mutations in the purine binding site exhibited the largest effects on enzymatic activity with the Asn243Ala mutant resulting in a 1000-fold decrease in the k_{cat} for inosine phosphorolysis. This result in combination with the crystallographic location of the Asn243 side chain suggested a potential transition state (TS) structure involving hydrogen bond donation by the carboxamido group of Asn243 to N7 of the purine base. Analogous to the oxyanion hole of serine proteases, this hydrogen bond was predicted to aid catalysis by preferentially stabilizing the TS as a consequence of the increase in negative charge on N7 that occurs during glycosidic bond cleavage and the associated increase in the N7−Asn243 hydrogen bond strength. Two residues in the phosphate binding site, namely His86 and Glu89, were also predicted to be catalytically important based on their alignment with phosphate in the X-ray structure and the 10−25-fold reduction in catalytic activity for the His86Ala and Glu89Ala mutants. In contrast, catalytic efficiencies for the Tyr88Phe and Lys244Ala mutants were comparable with wild-type, indicating that the hydrogen bonds predicted in the initial X-ray structure of PNP [Ealick, S. E., et al. (1990) *J. Biol. Chem. 265*, 1812−1820] were not essential for catalysis. These results provided the foundation for studies reported in the ensuing two manuscripts focused on the PNP catalytic mechanism [Erion, M. D., et al. (1997) *Biochemistry 36*, 11735−11748] and the use of mutagenesis to reverse the PNP substrate specificity from 6-oxopurines to 6-aminopurines [Stoeckler, J. D., et al. (1997) *Biochemistry 36*, 11749−11756].

Purine nucleoside phosphorylase (PNP, EC 2.4.2.1)[1] catalyzes the reversible phosphorolysis of purine nucleosides to generate the corresponding purine base and ribose 1-phosphate (Scheme 1) (Parks & Agarwal, 1972). In intact cells, phosphorolysis is favored due to the coupling of the PNP reaction with either purine base oxidation by xanthine oxidase or purine base phosphoribosylation by hypoxanthine-guanine phosphoribosyl transferase. Thermodynamically, however, nucleoside synthesis is favored over phosphorolysis with an equilibrium constant of approximately 50 for most purine nucleosides (Friedkin, 1950). Interest in PNP stems in large part from its potential as a drug target (Stoeckler,

Scheme 1

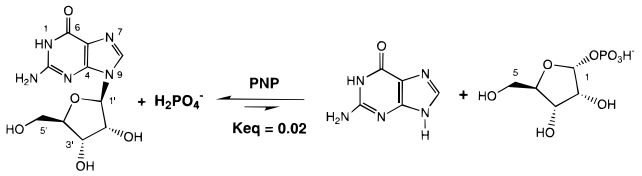

1984; Sircar & Gilbertsen, 1988; Ealick et al., 1991). The therapeutic utility of PNP inhibitors is based on the finding that PNP-deficient patients have little or no T-cell function but have a near-normal B-cell response (Giblett et al., 1975). Accordingly, PNP inhibitors are currently in development for T-cell mediated autoimmune reactions and T-cell leukemias. In addition, PNP inhibitors in combination with nucleoside antiviral and anticancer drugs have shown promise based on their ability to potentiate the in vivo activity of these drugs (Erion, 1990; Bennett et al., 1993).

Studies detailing PNP substrate specificity and catalysis have stimulated substantial interest in the use of PNP as a biocatalyst for the regio- and stereoselective synthesis of purine nucleosides (Krenitsky et al., 1981). Use of human PNP in enzymatic synthesis, however, is limited by its relatively narrow substrate specificity (Bzowska et al., 1990). For example, purines containing a 6-keto group, such as hypoxanthine and guanine, are strongly preferred over purines containing a 6-amino group, such as adenine (Zim-

† This work was supported by the National Institutes of Health to SEE (P01GM48874, P41RR01646, and CA67763). SEE is indebted to the W. M. Keck Foundation and the Lucille P. Markey charitable trust.

* Corresponding author: Gensia, Inc., 9360 Towne Centre Drive, San Diego, CA 92121. Telephone: (619) 622-4116; Fax: (619) 622-5545; E-mail: mark.erion@gensia.com.

‡ Ciba-Geigy Ltd.

§ Ciba-Geigy Corp.; present address: Genzyme Corp., Cambridge, Massachusetts.

|| Cornell University.

⊗ Abstract published in *Advance ACS Abstracts,* September 1, 1997.

[1] Abbreviations: PNP, purine nucleoside phosphorylase; XO, xanthine oxidase, INT, 2-(4-iodophenyl)-3-(4-nitrophenyl)-5-phenyltetrazolium chloride; HEPES, *N*-(2-hydroxyethyl)piperazine-*N*′-2-ethanesulfonic acid; DTT, dithiothreitol; PMSF, phenylmethanesulfonyl fluoride; IPTG, isopropylthiogalactoside; R1P, ribose 1-phosphate; TS, transition state; Hyp, hypoxanthine; Ino, inosine.

S0006-2960(96)01969-1 CCC: $14.00

merman et al., 1971). PNP is also specific for purine nucleosides in the β-configuration and exhibits a strong preference for ribosyl-containing nucleosides relative to the corresponding analogs containing the arabinose, xylose, or lyxose stereoisomers (Stoeckler et al., 1980).

Studies on the PNP catalytic mechanism have shown that PNP cleaves the glycosidic bond with inversion of configuration to produce α-ribose 1-phosphate (R1P). Analysis of the enzyme kinetics in the phosphorolysis direction indicated that catalysis occurs through a ternary complex of enzyme, nucleoside, and orthophosphate and that the kinetic mechanism for the multisubstrate reaction was ordered bi-bi with the base leaving after the ribose 1-phosphate (Krenitsky, 1967; Porter, 1992). Kinetic α-deuterium isotope effects indicated that bond breaking precedes bond making and thereby an S_N1-type mechanism (Stein & Cordes, 1981). Analyses of pH−rate profiles and the kinetics of chemically modified PNPs led to the postulation that an active-site histidine was involved in the deprotonation of phosphate to the more nucleophilic dianion and that a cysteine or lysine was involved in the protonation of the base to increase its leaving group ability (Jordan & Wu, 1978).

Recently, the X-ray structures for human PNP and several PNP−inhibitor complexes were solved at 2.75 and 3.2 Å resolution, respectively (Ealick et al., 1990, 1991). The crystal structures provided valuable insight into the origin of the high substrate specificity. For example, the high preference of PNP for 6-oxopurines relative to 6-aminopurines was apparent from the hydrogen bond pattern in the PNP-5′-iodoformycin B complex entailing hydrogen bonds between N1 and the carboxylate of Glu201 and between O6 and the active-site residues Lys244 and Asn243. The same structure also showed the sulfate positioned on the α-face of the ribose with one oxygen aligned for nucleophilic attack at C1′. This finding confirmed earlier kinetic studies indicating that glycosidic bond cleavage proceeded by an S_N1- or and S_N2-type mechanism and not by a mechanism involving enzyme intermediates.

The work reported herein and in the following two manuscripts was initiated in an effort to use the X-ray structure of PNP for the rational design of mutant PNPs with substrate specificities and catalytic properties useful for the large-scale synthesis of purine nucleoside analogs. Understanding the relationships between protein structure and both substrate binding and catalysis is important for the engineering of catalytically competent proteins with novel substrate specificities. Since the X-ray structure indicated that all direct contacts between PNP and the two substrates (purine nucleoside and phosphate) were through amino acid side-chains (Figure 1), we employed a site-directed mutagenesis strategy that resulted in replacement of each active-site residue with alanine in order to assess the contribution of the residue's side chain to substrate binding and catalysis. Results from the study led to a model of the transition state. Furthermore, these results in combination with results from crystallography, computer modeling and pseudosubstrate kinetics led to postulation of a catalytic mechanism (Erion et al., 1997) and to the design of PNP mutants that exhibit novel substrate specificities (Stoeckler et al., 1997).

MATERIALS AND METHODS

Materials. Purine nucleoside phosphorylase from human blood was purchased as a crude lyophilized powder from

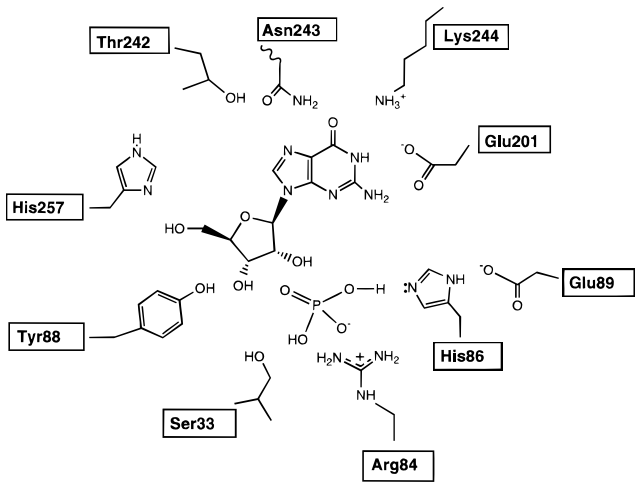

FIGURE 1: PNP active-site model constructed from the atomic coordinates for the PNP−guanine complex deposited in the Protein Data Bank (PNP4, Brookhaven National Laboratory).

Sigma. Xanthine oxidase from buttermilk was obtained from Fluka as a 60% saturated ammonium sulfate suspension. D-Ribose 1-phosphate was purchased with an estimated purity of 90% from Sigma. Inosine, hypoxanthine, HEPES, INT, Triton X-100, ammonium molybdate tetrahydrate, and sodium ascorbate were products of Fluka. Zinc acetate was obtained from Merck. Ampicillin, IPTG, DTT, and PMSF were products of Sigma. The pBR322-derived plasmid containing the gene for hPNP (pPNP) was kindly provided by Steve Williams (Genentech, San Francisco, CA). Enzymes for DNA manipulations were from Boehringer Mannheim.

Mutagenesis. Escherichia coli strains JM101 and XL-Blue (Stratagene) were used for isolation of double- and single-stranded DNAs, and CJ236 was used for isolation of uracil-containing single-stranded DNA. JM105 was used for expression of the gene for hPNP. *E. coli* DH5α was used as the initial cloning host for the pBR322-derived plasmid containing the hPNP gene (pPNP) (Williams et al., 1984). Digestion of the CsCl-gradient purified pPNP with *Kpn*I and *Hin*dIII yielded a 1 kb fragment containing the hPNP gene. Transfer of the fragment into the M13 mp19 vector and digestion with *Eco*RI and *Bam*HI yielded a 1.2 kb fragment. Transfer of this fragment into a pKK227-derived expression vector in which a synthetic ribosome binding site had been engineered (pPNP2), resulted in expression of the hPNP gene under control of the tac promoter.

Site-directed mutants of hPNP were prepared according to the method of Kunkel et al. (1987). The *Eco*RI/*Bam*HI fragment from pPNP2 was subcloned into pBluescript SK+ vector (Stratagene). After transformation of *E. coli* CJ236, uracil-containing single-stranded DNA was rescued with helper phage R408 (Stratagene). Mutations in the hPNP gene were introduced by annealing the uracil-containing single-stranded DNA with the corresponding altered oligonucleotides and then incubating the hybrid with T7 DNA polymerase and T4 ligase. The following oligonucleotides were synthesized on a DNA Synthesizer 380B (Applied Biosystems) according to the manufacturer's specifications

and used in the mutagenesis reactions.

S33A	5′ATC TGT GGT GCT GGA TTA3′
R84A	5′ATG CAG GGC GCG TTC CAC ATG3′
H86A	5′GGC AGG TTC GCC ATG TAT GAA3′
Y88F	5′TTC CAC ATG TTT GAA GGG TAC3′
E89A	5′CAC ATG TAT GCA GGG TAC CCA3′
F159A	5′TTT GGC GAT CGT GCC CCT GCC ATG3′
F200A	5′GGC CCC AGC GCT GAG ACT GT3′
E201A	5′CCA AGC TTT GCG ACT GTG GCA3′
M219A	5′GCT GTT GGC GCG AGT ACT GT3′
T242A	5′TCA CTG ATC GCT AAC AAG GTC3′
N243A	5′CTG ATC ACT GCC AAG GTC AT3′
K244A	5′TCA CTC ATC ACT AAC GCG GTC ATC ATG3′
H257A	5′AAG GCC AAC GCT GAA GAA GTC3′

The resulting heteroduplex DNA was transformed directly into *E. coli* JM101. To confirm the mutation, several colonies were picked and the plasmids sequenced by the dideoxy method (Sanger et al., 1977) using the Sequenase kit (U.S. Biochemical). The mutagenized *Eco*RI/*Bam*HI fragments were then spliced into the pKK227 expression vector and transformed into *E. coli* JM105.

Expression and Purification of Wild-type and Mutant hPNP. Starter cultures (5 mL) of *E. coli* JM105 cells harboring a plasmid containing the hPNP gene (wild-type or mutant) in LB medium containing 50 μg/mL ampicillin were grown overnight and used to inoculate 500 mL of fresh medium. The diluted cultures were grown at 37 °C to an absorbance (A_{600}) of ca. 0.2 and treated with IPTG (1 mM final concentration). After 4 h of additional growth, cells (∼0.5 g) were harvested by centrifugation (8000 rpm for 10 min in a Sorvall GSA rotor) at 4 °C, frozen in liquid nitrogen, and stored at −80 °C overnight. Cell pellets were suspended in 4 vol of 100 mM HEPES (pH 7.4), 2 mM DTT, and 0.5 mg/mL leupeptin and disrupted by sonication (Heat Systems-Ultrasonics, Inc.; 50% maximal power for 1 min). PMSF was added to a final concentration of 0.1 mM, and the sonication step was repeated two more times on ice. Cell lysates were diluted to 40 mL with 50 mM KH_2PO_4 (pH 7), 0.5 mM DTT, and 0.002% NaN_3 (henceforth designated as buffer B) and centrifuged at 7300*g* for 20 min at 4 °C to remove cell debris. The resulting crude extracts (∼40 mL) were added to an equal volume of red A agarose (Amicon) that had been thoroughly prerinsed with buffer B. After gently stirring on ice for 30 min, the red A agarose slurries were drained on disposable filter units and rinsed with 200 mL of buffer B. Absorbed material was then eluted in two fractions by rinsing the slurries in succession with 200 mL of buffer B containing 0.25 M NaCl and then 200 mL of buffer B containing 1.0 M NaCl. Eluates from the latter rinse were concentrated to 5 mL by ultrafiltration (Amicon Ultrafiltration Cell Models 8400 and 8050) and desalted by two cycles of dilution to 50 mL with 25 mM imidazole (pH 7), 0.5 mM DTT, and 0.002% NaN_3 (henceforth designated buffer C). The final 5 mL concentrate was applied to an FPLC Mono P HR 5/20 column (Pharmacia) pre-equilibrated with buffer C. The column was rinsed with 10 mL of buffer C, and chromatofocusing was initiated by elution with Polybuffer 74 (Pharmacia) diluted 1:10 with 50 mM NaCl, 0.5 mM DTT, and 0.002% NaN_3. Fractions (1 mL) were analyzed for protein and PNP activity. Protein concentrations were determined by the Bradford protein assay (Bradford, 1976) using reagents from Bio-Rad and BSA as the standard. PNP activity was determined using the coupling assay of Kalckar (1947). Specifically, uric acid production was monitored at 293 nm in assay solutions containing 50 mM KH_2PO_4 (pH 7.0), 5 mM inosine, and 0.04 unit/mL xanthine oxidase. One unit of PNP is defined as the amount of PNP required to phosphorolyze 1 μmol of inosine/min. Fractions with the highest specific activities were pooled and concentrated to ≥1 mg/mL using an Amicon Centricon 10. The buffer was then exchanged with the storage buffer B by two cycles of dilution and reconcentration. The final protein solution was stored directly or as a 1:1 buffer B:PEG solution at −78 °C. PNP activity was reassayed prior to kinetic analysis to confirm that no activity was lost during long term storage or the freeze−thaw step.

Assay of PNP Phosphorolysis Activity. Inosine phosphorolysis was assayed in microtiter plate format using a BIOMEK workstation (Beckman) to dispense the reagents and the BIOMEK optical density tool or the Dynatech MR5000 multiwell reader to monitor the absorbance changes at 490 nm. Assay linearity was assessed with respect to time and enzyme concentration using assay mixtures (200 μL) incubated at 25 °C and consisting of 100 mM HEPES (pH 7.0), 1 mM inosine, 50 mM potassium phosphate (pH 7.0), 0.075% Triton X-100, 1 mM 2-(4-iodophenyl)-3-(4-nitrophenyl)-5-phenyltetrazolium chloride (INT), 20 munits (milliunits) of xanthine oxidase, and 0−2.2 munits of PNP. Substrate kinetic parameters were determined from initial velocity data generated at a fixed concentration of inosine or KH_2PO_4 (>10 times the K_M value for the given PNP mutant) and a concentration of the other substrate that varied over a minimum of a 10-fold concentration range. A preliminary activity test was conducted on each mutant to select an appropriate range of inosine concentrations for determination of the K_M at 50 mM phosphate. The K_M for phosphate was subsequently determined from assay results generated by varying the phosphate concentration (0.5−50 mM) and holding the inosine concentration fixed at ≥10 K_M. Assays were repeated when the calculated K_M value for the substrate with variable concentrations was not bracketed by the substrate concentrations used in the assay.

Assay of PNP Nucleoside Synthesis Activity. Rates of PNP-catalyzed inosine synthesis from hypoxanthine and ribose 1-phosphate were determined at single time points using a colorimetric assay for inorganic phosphate (Saheki et al., 1985). The assay was configured to a microtiter plate format using a BIOMEK workstation to dispense the reagents as well as to initiate and quench the reaction. Assay linearity was assessed with respect to time and enzyme concentration using assay mixtures (100 μM) containing 100 mM HEPES (pH 7.0), 4 mM ribose 1-phosphate, 0.2 mM hypoxanthine, 0.075% Triton X-100, and 0−2.2 munits of PNP. Reactions were initiated with either PNP or R1P and quenched simultaneously at the indicated time (e.g., 1.5 min) by the addition of 80 μL of a solution of 200 mM zinc acetate and 30 mM ammonium molybdate (pH 5.0). A 20% solution of ascorbic acid (20 μL, pH 5.0) was added immediately thereafter in accordance with the published procedure. The absorbance of the resulting zinc-dependent phosphomolybdate complex was measured at 850 nm with a Dynatech MR5000 multiwell reader. Color development was monitored at 1 min intervals and automatically evaluated for maximal color development and stability. After full color development (ca. 20 min), absorbance values were corrected

by subtracting background absorbance values derived from companion assay solutions lacking either PNP or hypoxanthine. Absolute phosphate concentrations were determined from a standard curve. The substrate kinetic parameters for nucleoside synthesis with PNP were determined by varying the concentration of hypoxanthine in the presence of 4 mM R1P and by varying the concentration of R1P in the presence of 0.5 mM hypoxanthine. A preliminary activity test was conducted on each mutant PNP to select an appropriate range of hypoxanthine concentrations for determination of the K_M.

Determination of Kinetic Parameters. All enzyme reactions were performed in triplicate at 25 °C. Kinetic parameters were determined from Lineweaver−Burk plots of initial velocity data generated for seven substrate concentrations. K_M and k_{cat} values were obtained from nonlinear regression analysis of data fitted to the Michaelis−Menten equation with the Enzfitter computer program (BIOSOFT-Elsevier). Calculations of k_{cat} were based on a subunit molecular mass of hPNP of 32 000 Da. Standard errors were in the same range as reported in the following manuscripts in this issue (Erion et al., 1997; Stoeckler et al., 1997).

RESULTS

Isolation and Characterization of PNPs. Overexpression of the wild-type PNP and mutant PNPs in *E. coli* by the procedures described in the Materials and Methods led to cell homogenates in which PNP represented greater than 5% of the soluble protein. Although strains of *E. coli* that lack bacterial PNP activity were available (Jochimsen et al., 1975) and on occasion used, DH5α and JM105 *E. coli* were selected as expression hosts due to their enhanced viability. Use of these hosts was possible because the two-step purification procedure (Table 1) completely separated the constitutively produced bacterial PNP (bPNP) from the recombinant human PNP (approximate intracellular ratio of hPNP to bPNP = 22:1). Separation was achieved by using the dye-matrix resin red A agarose. Under low ionic strength conditions, the bacterial enzyme did not bind to the resin whereas the human PNP was tightly bound. This difference in binding affinity for red A agarose was confirmed by expression of hPNP in an *E. coli* mutant strain that completely lacks bacterial PNP activity (Sϕ312). In this case, no PNP activity was observed in the low ionic strength washes (data not shown), suggesting that hPNP bound tightly to the resin and that the separation between bPNP and hPNP was large. The overall purification of hPNP resulting from the dye-matrix was approximately 6-fold (Table 1). Further purification of wild-type and mutant PNPs was accomplished by chromatofocusing on a Mono P column. In contrast to the red A agarose step, human PNP eluted in the low ionic strength buffer (50 mM NaCl) whereas the bacterial PNP bound tightly to the Mono P column under these conditions and required 1 M NaCl for elution. Overall a 22-fold purification was achieved by the two-step procedure. Analysis of the protein purity by SDS−PAGE confirmed that the PNPs purified by the two-step procedure were full-sized polypeptides and essentially homogeneous (Figure 2). In some cases, a minor band was observed. Western blot analyses (data not shown) using a polyclonal rabbit anti-human PNP antibody (Goddard et al., 1983) indicated that the minor contaminant was possibly related to PNP.

The structural integrity of the PNP mutants was evaluated in two ways. First, the mobilities of the mutant proteins were evaluated by PAGE under nondenaturing conditions. Analysis of the gel indicated that all thirteen mutants exist as the expected trimer (data not shown). In addition, the different mobilities among the mutant proteins were consistent with the intended substitutions. Substitution of Arg84 or Lys244 with alanine resulted in proteins with correspondingly enhanced mobilities. Likewise, replacement of Glu89 or Glu201 yielded proteins with retarded mobilities. Because the native gels were run at a pH of 8.5, the mobilities of the Tyr88Ala, His86Ala, and His257Ala mutant proteins were not significantly altered relative to the wild-type enzyme. The second method used to monitor the structural integrity of the mutant proteins involved K_M determinations for phosphate for purine binding site mutants and correspondingly K_M determinations for hypoxanthine for both phosphate binding site and ribose binding site mutants. Large deviations in the K_M values for the mutant protein relative to the wild-type enzyme were considered potential indicators for mutation-induced structural changes. Of the 13 mutants analyzed, only the Thr242Ala mutation produced a significant effect on the K_M for the "control" substrate.

Table 1: Purification of hPNP from *E. coli* JM105

purification step	protein (mg)	specific activity (units/mg)	purification fold	yield (%)
crude extract	68	3.3	1	100
red A agarose	8.5	20.2	6	76
Mono P	1.3	72.9	22	42

Phosphorolysis Assay. Simple addition of INT (DeGroot et al., 1985) to the previously reported xanthine oxidase-coupled assay (Kalckar, 1947) resulted in the formation of the highly colored formazan product ($\epsilon = 1.2 \times 10^4$ M^{-1} cm^{-1}; $\lambda = 490$ nm). Analysis of the reaction indicated, however, that the progress curves were nonlinear due to slow precipitation of formazan. Addition of Triton X-100, while having no effect on the overall enzyme activity, decreased the rate of formazan precipitation at 25 °C and led to linear progress curves. Linearity was maintained for at least 10 min and in some cases for as long as 60 min provided that the A_{490} did not exceed 2.0 absorbance units. In addition, these conditions were shown to produce initial velocities that were linearly dependent on PNP concentration over a 50-fold range (data not shown).

Linear double reciprocal plots of initial velocities and substrate concentration were obtained for both inosine (Figure 3A) and phosphate (data not shown) using human PNP in the colorimetric assay. Linear plots were also obtained for PNP mutants. In general, a relatively narrow substrate concentration range (10−50-fold) was chosen for the variable substrate (see Materials and Methods) since previous work had shown significant nonlinearity when a broad range of phosphate concentrations was evaluated with calf spleen PNP (Ropp & Traut, 1991). A subsequent report indicated that linearity was maintained when phosphate concentrations were below 30 μM or above 200 μM (Porter, 1992). Nonlinear kinetics have also been observed at high nucleoside concentrations (e.g., 2′-deoxyinosine) with human erythrocytic PNP (Kim et al., 1968; Agarwal et al., 1975) and in some cases with the recombinant enzyme. This failure to obey Michaelis−Menten kinetics has been attributed to nonequivalent active sites (Parks & Agarwal, 1972) or to a substrate-induced dissociation of the trimer into monomers (Ropp & Traut, 1991). Accordingly, initial velocity data was gathered in these studies using phosphate concentrations

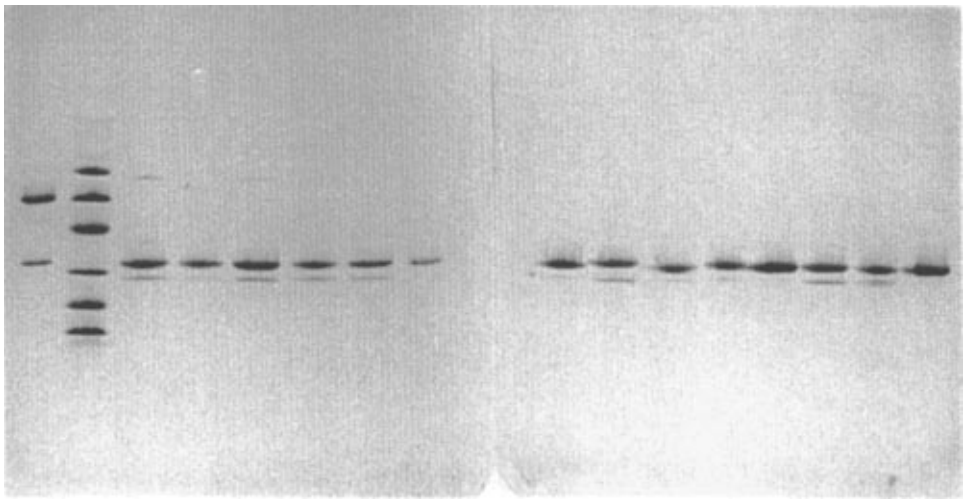

FIGURE 2: Electrophoretic mobilities of hPNP variants in the presence of sodium dodecyl sulfate. Lane 1, erythrocytic hPNP (Sigma). Lane 2, molecular mass standards: phosphorylase b (92.5 kDa), bovine serum albumin (66.2 kDa), ovalbumin (45 kDa), carbonic anhydrase (31 kDa), soybean trypsin inhibitor (21.5 kDa), and lysozyme (14.4 kDa). Lanes 3−16, PNP mutants: lane 3, Ser33Ala; lane 4, Arg84Ala; lane 5, His86Ala; lane 6, Tyr88Phe; lane 7, Glu89Ala; lane 8, Phe159Ala; lane 9, wild-type recombinant hPNP; lane 10, Phe200Ala; lane 11, Glu201Ala; lane 12, Met219Ala; lane 13, Thr242Ala; lane 14, Asn243Ala; lane 15, Lys244Ala; lane 16, His257Ala.

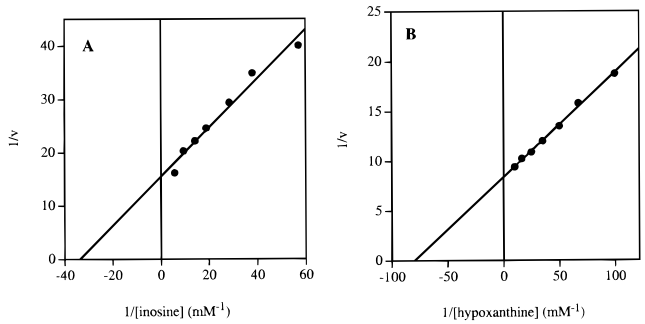

FIGURE 3: Lineweaver−Burk plots of initial velocities for the phosphorolysis reaction (A) and synthesis reaction (B) using erythrocytic hPNP (Sigma). In the phosphorolysis reaction, the phosphate concentration was fixed at 50 mM. In the synthesis reaction, the ribose 1-phosphate concentration was fixed at 4 mM and the reactions were quenched after 2 min. Initial velocities were determined from absorbance values and a standard curve. (see Materials and Methods for details). The calculated K_M values for inosine and hypoxanthine were 29 ± 3 and 12 ± 1 μM, respectively.

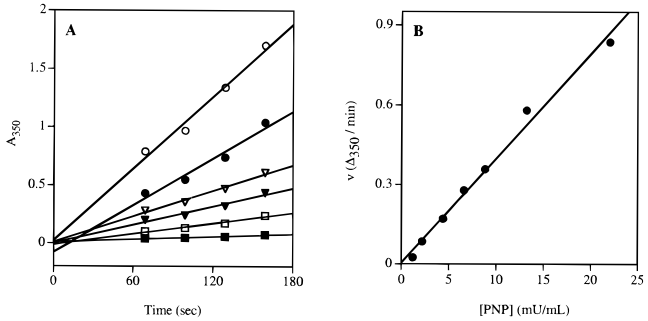

FIGURE 4: Linearity of PNP activity in colorimetric assay for nucleoside synthesis using erythrocytic hPNP (Sigma). (A) Progress curves obtained for reactions (100 μL) containing 22 (○), 13.2 (●), 8.8 (▽), 6.6 (▼), 4.4 (□) or 2.2 (■) munits/mL PNP were carried out as described in Materials and Methods and quenched at the indicated time points by addition of the zinc acetate/ammonium molybdate solution. (B) Plot of reaction rates calculated from assays quenched at 1.5 min vs PNP concentration.

which ranged between 0.5 and 50 mM and inosine concentrations that did not greatly exceed 10 K_M. Under these conditions, k_{cat} and K_M values determined for inosine phosphorolysis with the wild-type enzyme using the microtiter plate assay were identical to the values determined from data generated using the Kalckar method (data not shown; Bzowska et al., 1990). Furthermore, similar results were obtained for the wild-type enzyme and for the PNP mutants Asn243Ala and Glu201Ala using a radiolabelled assay (Stoeckler et al., 1997).

Nucleoside Synthesis Assay. Numerous methods exist for the detection of inorganic phosphate. The most sensitive methods involve the formation of a highly colored phosphomolybdate complex under strongly acidic conditions (Lanzetta et al., 1979). These methods were not suitable for PNP, however, due to the hydrolytic lability of ribose 1-phosphate at low pH. One method for determining phosphate concentrations at pH 5.0 was reported to have a sensitivity within the range required for study of PNP-catalyzed nucleoside synthesis (Saheki et al., 1985). Under these assay conditions, the rate of ribose 1-phosphate hydrolysis (0.003 OD/min at 2 mM ribose 1-phosphate) was slow relative to the rate of phosphate production via nucleoside synthesis and the time required for development of the phosphate-dependent chromophore (ca. 20 min).

Evaluation of the time course of the reaction showed that the progress curve was linear for at least 3 min over a 10-fold range of PNP concentrations (Figure 4A). These conditions also resulted in a linear dependence of the initial velocities on PNP concentration (Figure 4B). Linear double reciprocal plots were obtained when hypoxanthine (Figure 3B) and R1P (data not shown) concentrations were varied. The K_M for hypoxanthine and ribose 1-phosphate as determined from these plots (12 and 290 μM, respectively) are in good agreement with values reported in the literature (Parks & Agarwal, 1972; Stoeckler & Parks, 1985). Concentrations of ribose 1-phosphate higher than 4 mM were not used due to the background rate of phosphate production relative to the rate of nucleoside synthesis. Consequently the k_{cat} for synthesis may represent an underestimation of the true value due to nonsaturating ribose 1-phosphate concentrations for PNP mutants that have an increased ribose 1-phosphate K_M.

Mutant PNP Kinetics. PNP mutants were loosely divided into three groups based on the crystallographic placement of the active-site residue with respect to the substrates (Figure 1). Residues targeted for mutagenesis formed either a

Table 2: Kinetic Parameters of Purine Subsite Mutants

enzyme	substrate	K_M (mM)	k_{cat} (s^{-1})	k_{cat}/K_M[a] ($s^{-1}\,M^{-1}$)
PNP (wt)	Ino	0.040	56	1.4
	Pi	4.0	56	0.014
	Hyp	0.030	110	3.7
E201A	Ino	8.4	4.2	0.0005
	Pi	6.1	1.8	0.0001
	Hyp	1.0	1.4	0.001
N243A	Ino	0.022	0.06	0.003
	Pi	3.5	0.09	0.000 03
	Hyp	2.3	13	0.006
K244A	Ino	0.037	49	1.3
	Pi	2.7	52	0.019
	Hyp	0.040	98	2.5
F200A	Ino	19	9.4	0.0005
	Pi	4.5	6.2	0.001
	Hyp[b]	0.57	14	0.024
T242A	Ino	0.022	14	0.64
	Pi	0.22	12	0.06
	Hyp	0.024	58	2.4

[a] $\times 10^6$. [b] Kinetic values determined at 4 mM ribose 1-phosphate concentration.

Table 3: Kinetic Parameters of Ribose Subsite Mutants

enzyme	substrate	K_M (mM)	k_{cat} (s^{-1})	k_{cat}/K_M[a] ($s^{-1}\,M^{-1}$)
PNP (wt)	Ino	0.040	56	1.4
	Pi	4.0	56	0.014
	Hyp	0.030	110	3.7
H257A	Ino	0.21	16	0.07
	Pi	2.5	13	0.005
	Hyp[b]	0.020	10	0.50
F159A	Ino	0.31	32	0.10
	Pi	2.5	30	0.01
	Hyp[b]	0.025	24	1.0
M219A	Ino	8.0	52	0.01
	Pi	4.3	41	0.01
	Hyp[b]	0.18	130	0.72
Y88F	Ino	0.058	54	0.93
	Pi	2.1	56	0.03
	Hyp[b]	0.010	9.0	0.90

[a] $\times 10^6$. [b] Kinetic values determined at 4 mM ribose 1-phosphate concentration.

hydrogen bond or a van der Waals contact directly with a substrate or with a residue that interacted with a substrate. Accordingly, five residues in the purine binding site, four residues in the ribose binding site, and four residues in the phosphate binding site were mutated to alanine in order to assess the importance of each individual contact on substrate binding and catalysis. Each mutant was assayed in both directions to determine the k_{cat} and the K_M values for inosine, phosphate, and hypoxanthine. In general, mutations in the purine binding sites exhibited a K_M for phosphate similar to wild-type whereas mutations in the phosphate binding site exhibited a K_M for hypoxanthine similar to wild-type. Kinetic parameters determined for the mutant proteins are summarized in Tables 2−4.

Purine Binding Site Mutants. Kinetic data for each purine binding site mutant are shown in Table 2. The largest effects were observed for the Asn243, Glu201 and Phe200 mutants. In the phosphorolytic direction, the primary effect of mutation of Phe200 and Glu201 was a 200−400 fold increase in the K_M for inosine whereas mutation of Asn243 led to a 1000-fold decrease in k_{cat}. Little effect was observed on the K_M for phosphate, suggesting that these mutations do not produce large structural perturbations at the active site. In the synthetic direction, the primary effect of the Asn243 mutation was on the K_M for hypoxanthine, which increased 77-fold whereas k_{cat} decreased only 8.5-fold. The decrease in k_{cat}/K_M for the Asn243Ala mutant was therefore approximately the same for the phosphorolytic (470-fold) and synthetic (620-fold) directions. The Glu201Ala mutant proved to be a less efficient enzyme relative to wild-type and the Asn243Ala mutant with the k_{cat}/K_M value decreased relative to wild-type by 3700-fold in the synthesis direction and by 2800-fold in the phosphorolytic direction. Unlike the Asn243Ala mutant, the decrease in efficiency was due to effects on both k_{cat} and K_M. In contrast to these mutants, the Lys244Ala mutant exhibited kinetics similar to the wild-type enzyme. The Thr242Ala mutant also exhibited kinetics similar to wild-type with the exception of its decreased K_M for phosphate. The hydroxyl of Thr242 appears to be important in this effect, since the Thr242Ser mutant has a K_M for phosphate similar to wild-type (data not shown).

Ribose Binding Site Mutants. The four residues in the ribose binding site subjected to mutagenesis were His257, Met219, Tyr88, and Phe159. In this study, Tyr88 was converted to phenylalanine whereas the other three residues were replaced with alanine. Kinetic data for each ribose binding site mutant are shown in Table 3. Analysis of the Tyr88Phe mutant showed no significant differences in K_M or k_{cat} compared to wild-type PNP in the phosphorolysis direction. In the synthesis direction, a 4-fold decrease in catalytic efficiency was observed, possibly suggesting that the Tyr88-O3′ interaction may be more important for binding ribose 1-phosphate or that the ribose 1-phosphate concentration was not saturating. Kinetic data for the Met219Ala and Phe159Ala mutant reflect little change in k_{cat} whereas the K_M increased 5−100-fold. In contrast, the His257Ala mutant showed a rather modest 20-fold decrease in k_{cat}.

Phosphate Binding Site Mutants. The four residues in the phosphate binding site subjected to mutagenesis were Arg84, His86, Ser33, and Glu89. Crystallographic studies indicated that phosphate (sulfate in the crystal structure) participates in a number of ionic and hydrogen bond interactions. Crystallographic studies also revealed a previously unrecognized structural arrangement between phosphate, His86, and Glu89 reminiscent of the serine protease catalytic triad (Ser-His-Asp). Kinetic data for each phosphate binding site mutant are shown in Table 4. Mutations in residues that directly contact phosphate led to a decrease in catalytic efficiency ranging from 25- to 185-fold. Surprisingly, the decrease in catalytic efficiency was not a reflection of a higher phosphate K_M, but rather of a decrease in k_{cat}. For example, replacement of the positively charged Arg84 side-chain with alanine led to a mutant that exhibited a K_M for phosphate and hypoxanthine identical to wild-type and a K_M for inosine 3-fold higher than wild-type. In comparison, the Arg84Ala mutant showed a 50- and 200-fold decrease in k_{cat} for phosphorolysis and synthesis, respectively. In addition to residues that directly contact phosphate, Glu89 was studied in order to assess the potential role of the His86−Glu89 diad in catalysis. As shown in Table 4, the Glu89Ala mutant exhibited a 20-fold increase in the K_M for phosphate whereas no effect was observed on k_{cat} in the phosphorolysis direction.

In the synthetic direction, several mutants exhibited a large reduction in k_{cat} (e.g., 110-fold for His86Ala), which could suggest a large role for these residues in the transition state (TS) used for nucleoside synthesis. Some caution, however, is required for conclusions based on the kinetics of either phosphate or ribose binding site mutants, since the mutations

Table 4: Kinetic Parameters of Phosphate Subsite Mutants

enzyme	substrate	K_M (mM)	k_{cat} (s^{-1})	k_{cat}/K_M[a] (s^{-1} M^{-1})
PNP (wt)	Ino	0.040	56	1.4
	Pi	4.0	56	0.014
	Hyp	0.030	110	3.7
H86A	Ino	0.28	14	0.05
	Pi	9.2	9.4	0.0008
	Hyp[b]	0.019	0.97	0.05
E89A	Ino	0.22	46	0.21
	Pi	91	53	0.0006
R84A	Ino	0.13	2.1	0.016
	Pi	4.5	1.5	0.0003
	Hyp[b]	0.020	0.5	0.025
S33A	Ino	0.14	11	0.08
	Pi	3.6	11	0.003
	Hyp[b]	0.013	2.1	0.15

[a] $\times 10^6$. [b] Kinetic values determined at 4 mM ribose 1-phosphate concentration.

may also cause a large increase in the K_M for ribose 1-phosphate and lead to an underestimation of k_{cat}. Unfortunately, concentrations of ribose 1-phosphate higher than the standard assay concentration of 4 mM (K_M for wild-type = 290 μM) were not possible due to an unacceptably high background rate resulting from chemical hydrolysis.

DISCUSSION

PNP Activity Assays. To determine the kinetic parameters for a large number of PNP mutants with a variety of structurally diverse substrates, we needed PNP assays that were high throughput and capable of monitoring phosphorolysis and nucleoside synthesis activity with few restrictions on the substrate structure. Although numerous PNP assays have been reported in the literature (Stoeckler, 1985), none were suitable for our purposes. Highly sensitive assays using radiolabeled substrates (Chang et al., 1989) were too labor intensive and not readily applicable to analysis of pseudosubstrate kinetics. Assays designed to monitor turnover by detecting the products spectrophotometrically were relatively insensitive and limited to purines in which the purine nucleoside and purine base had sufficiently different absorption maxima. Furthermore, these assays were not applicable to phosphorolysis due to the unfavorable equilibrium constant. To circumvent the latter complication, a coupled assay using xanthine oxidase is often used to monitor phosphorolysis (Kalckar, 1947). The limitations inherent to this assay, however, include the difficulty in monitoring reactions at 293 nm on a microtiter plate and the inability to use potential pseudosubstrates that lack hypoxanthine as the base.

The two microtiter plate assays developed for monitoring nucleoside phosphorolysis and nucleoside synthesis gave results consistent with the previously reported PNP assays. The microtiter plate assays, however, have the advantage of speed and automation as well as the ability to evaluate a wide variety of substrate analogs under a single set of conditions. This is especially true for the nucleoside synthesis assay, since monitoring phosphate production is independent of the purine base and substituents on the ribose 1-phosphate.

Substrate Binding. Crystal structures of PNP complexes identified the active-site residues in contact with the purine nucleoside and the phosphate (Figure 5). Changes in substrate affinity were assumed to be qualitatively reflected by the changes in K_M based on the similarity in the inosine K_M value and the apparent dissociation constant for the calf

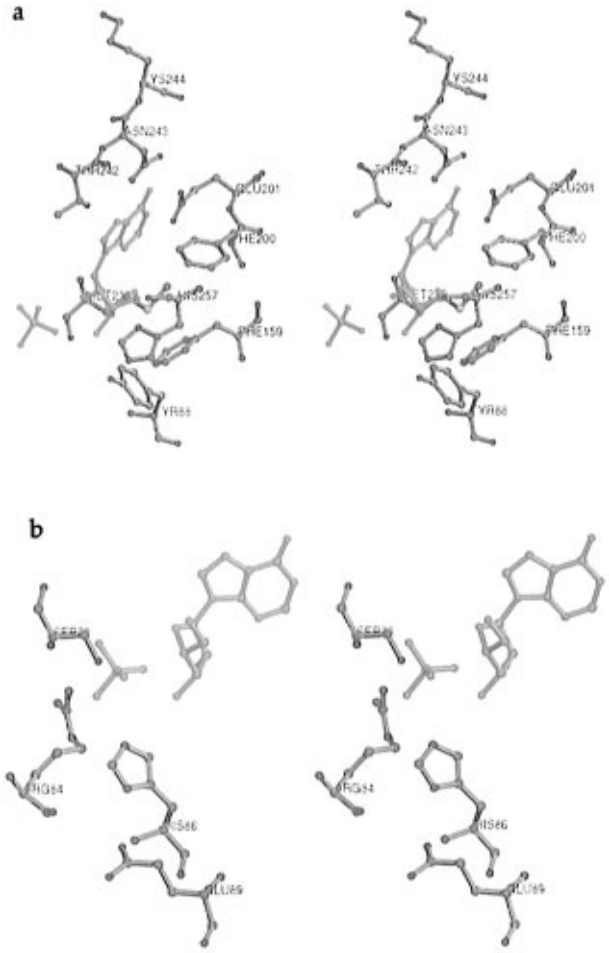

FIGURE 5: Three-dimensional structure of human PNP active-site based on the refined atomic coordinates. Panel A (top) shows a stereoplot of the active site centered at the nucleoside binding site. Panel B (bottom) shows a stereoplot of the phosphate binding site.

spleen PNP−inosine complex (Kline & Schramm, 1992). Results from the kinetic studies indicated that substrate binding was most sensitive to mutations in the purine binding site followed by mutations in the ribose and then phosphate binding sites (Tables 2−4).

Initial crystallographic studies indicated that the side chains of Lys244, Asn243 and Glu201 form hydrogen bond contacts with O6 and N1 of the purine base (Ealick et al., 1990). Molecular modeling studies indicated that a hydrogen bond between Asn243 and N7 was also possible, although not readily apparent in the X-ray structure based on the distance between the corresponding heteroatoms as well as the projected hydrogen bond angle. The predicted hydrogen bond between the ϵ-amino group of Lys244 and O6 was derived from molecular modeling studies, since electron density was not detected for the Lys244 side-chain atoms beyond the β-carbon. The remaining atoms in the side chain were therefore positioned after analysis of potential side-chain conformations and the identification of one low energy conformer that placed the ϵ-amino group in hydrogen bond contact with O6. The X-ray structure also indicated that Phe200 and Ala116 contact the two faces of the purine base with the Phe200 side-chain phenyl group making a classic herringbone-type interaction with the base.

Of the four residues that contact the purine base, only the Lys244Ala mutant exhibited kinetics similar to the wild-type enzyme. This result led to further scrutiny of the PNP structure and to the position of the Lys244 side chain.

Subsequent refinements in the X-ray structure resulted in the reorientation of the Lys244 side chain such that it is now pointing away from the active site and into solvent (unpublished results). These results are consistent with the side-chain positions predicted for the two preceding residues, i.e., Asn243 and Thr242, since both point into the active site thereby making it unlikely that the Lys244 side chain also points into the active site based on normal main-chain torsion angles. These results do not preclude, however, the possibility that the Lys244 side chain points into the active site and participates in a salt bridge with Glu201 and then swings out toward the solvent upon ligand binding.

In contrast to Lys244, replacement of Asn243, Glu201, and Phe200 with alanine led to large decreases in catalytic efficiencies (500−2800-fold). The decrease in phosphorolytic activity for the Glu201 and Phe 200 mutations was due to changes in both k_{cat} and K_M, but predominantly K_M. The large decrease in substrate affinity for the Glu201 and Phe200 mutants is consistent with the interactions indicated by the X-ray structure. In the case of Glu201, one oxygen of the side-chain carboxyl forms a hydrogen bond with the N1 hydrogen while the second oxygen is available to form a hydrogen bond with the 2-amino group of guanine. Accordingly, the carboxylate appears to exist as the carboxylic anion based on the hydrogen bond pattern and the pK_a of glutamate residues. Since hydrogen bonds to charged groups in relatively hydrophobic environments can contribute significant binding energy (∼4−5 kcal/mol; Fersht et al., 1985), the 210-fold increase in K_M for the Glu201Ala mutant is within expectation. A similar increase in K_M was observed for the Phe200Ala mutant, which reflects the loss in the herringbone-type interaction. Given that this type of interaction is considerably weaker than that expected for a N1−Glu201 hydrogen bond, the loss in substrate affinity may also imply some additional structural perturbations.

Unlike the Glu201Ala and Phe200Ala mutants, the large decrease in phosphorolytic efficiency exhibited by the Asn243Ala mutant relative to wild-type was not as a result of an increase in K_M for inosine but rather to a 1000-fold decrease in k_{cat}. Crystallographic studies of PNP complexed with purine bases or purine nucleoside analogs revealed several possible Asn243 side-chain orientations and corresponding hydrogen bond interactions between the Asn243 carboxamido group and both the purine base (N7 and O6) and the side-chain hydroxyl of Thr242 (Figure 5A). For example, X-ray structures of PNP complexes with 9-deazapurine analogs showed the carbonyl of the carboxamido group to accept a hydrogen bond from the N7-hydrogen (Figure 6A). In contrast, X-ray structures of PNP complexed to purine analogs resistant to hydrolysis indicated that the carbonyl accepts a hydrogen bond from Thr242 while the Asn243 amido group donates a strong hydrogen bond to O6 and a weak hydrogen bond to N7 (Figure 6B). Attempts to determine the X-ray structure of PNP complexed with either inosine or guanosine failed due to their instability to the crystal soaking conditions. Recent refinements in the X-ray structure and molecular modeling studies (Erion et al., 1997) suggest that the carboxamido group may be rotated 180° from the PNP−9-deazaguanine structures such that the amido group forms a weak hydrogen bond to N7 ∼3.2 Å for bovine PNP) while donating a hydrogen bond to Thr242 (Figure 6C). This configuration would suggest that the carbonyl oxygen makes a van der Waals contact with O6. These results are further supported by the bovine PNP structure, which was solved recently at 1.8 Å resolution (Mao, C., & Ealick, S. E., unpublished results). The absence of a strong hydrogen bond between Asn243 and the purine nucleoside in the latter hydrogen bond pattern is consistent with the lack of an effect on the K_M value for inosine upon mutation of Asn243 to alanine.

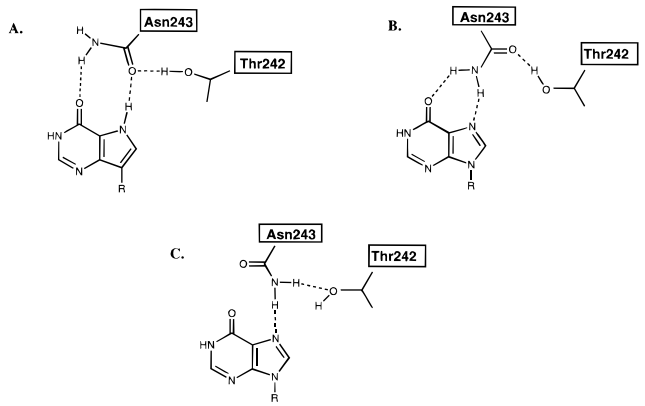

FIGURE 6: Hydrogen bond patterns predicted from X-ray data: (A) pattern predicted for 9-deazapurines using coordinates from PNP−inhibitor complexes (Ealick et al., 1991); (B) pattern for purines predicted from active-site modeling studies using the original atomic coordinates (Ealick et al., 1990); and (C) pattern predicted from refined atomic coordinates.

In the synthesis direction, the Asn243Ala mutant exhibited an 80-fold increase in the hypoxanthine K_M relative to wild-type. This result implies that the carboxamido group of Asn243 is important for substrate binding in nucleoside synthesis and for catalysis in the phosphorolysis reaction. The larger effect of the Asn243 mutation on the hypoxanthine K_M relative to the inosine K_M suggests that the carboxamido group forms a significantly stronger hydrogen bond with the purine base. Since nucleoside synthesis likely entails reaction of a negatively charged purine base with ribose 1-phosphate, the difference in K_M may be due to a hydrogen bond between the carboxamido group and a negatively charged N7 based on the increased hydrogen bond strength predicted for hydrogen bonds formed between donors and charged acceptors.

Purine nucleoside binding and specificity is also determined by residues in the ribose binding site. X-ray structures of a variety of PNP complexes indicated that PNP interacts with the ribose moiety through hydrogen bonds between the phenolic group of Tyr88 and O3′ and between the imidazole of His257 and O5′. In addition, the β-face of the ribose forms van der Waals contacts with the side chains of Met219 and Phe159. Mutation of Tyr88 to Phe had little effect on the K_M for inosine, suggesting that the hydrogen bond to O3′ was not important for inosine binding. This result was somewhat surprising given the poor overall activity reported for 3′-deoxyinosine and its corresponding 40-fold higher K_M (Stoeckler et al., 1980). Since X-ray data also indicated that the O3′-hydroxyl forms a hydrogen bond to phosphate, the poor activity of 3′-deoxyinosine might be attributed to the lack of this interaction, which could be important in the alignment of the phosphate for either TS stabilization or nucleophilic attack at C1′.

Replacement of His257, Phe159, and Met219 with alanine led to mutants with higher K_M values for inosine. The largest effects were observed for the Phe159 and Met219 alanine mutants, suggesting that the interaction between the β-face of the ribose and the hydrophobic surface created by these

residues is important for substrate binding. On the other hand, the modest 5-fold increase in K_M for the His257Ala mutant suggested that the hydrogen bond observed between the His257 imidazole and the O5′-hydroxyl was not essential for nucleoside binding. This conclusion was supported by earlier kinetic studies which showed 5′-deoxyinosine and inosine to have similar kinetic parameters (Stoeckler et al., 1980).

In contrast to ribose, phosphate forms multiple ionic and hydrogen bond contacts with PNP. Most of the contacts are through hydrogen bonds with the exception of two ionic interactions involving Arg84 and His86. Alanine mutants of these residues showed no increase in the phosphate and hypoxanthine K_M values and a 3−7-fold increase in the K_M for inosine. The lack of an effect on the phosphate K_M may just reflect the fact that phosphate binding involves many interactions and that no one interaction strongly affects phosphate binding affinity. Interestingly, the one mutant that exhibited a large increase in the K_M for phosphate was the Glu89Ala mutant. Since Glu89 interacts with phosphate indirectly through the His86 imidazole, the 20-fold increase in the K_M may reflect a misalignment of the His86 imidazole group and a resulting unfavorable interaction with phosphate.

Catalysis. Analysis of α-secondary deuterium kinetic isotope effects for the phosphorolysis (Stein & Cordes, 1981) and arsenolysis (Kline & Schramm, 1993) of inosine indicated that the PNP-catalyzed reaction follows an S_N1-type mechanism with a TS having considerable oxocarbenium ion character. On the basis of this prediction and the mechanism reported for other glycosidic bond-cleaving enzymes, PNP was expected to have carboxylic acid-containing residues near N7 of the purine base and near the ribosyl oxygen. The carboxylic acid near N7 was expected protonate N7 and thereby facilitate glycosidic bond cleavage in a manner analogous to the mechanism reported for acid-catalyzed purine nucleoside hydrolysis (Zoltewicz et al., 1970). The carboxylic acid near the ribosyl oxygen was expected to stabilize the oxocarbenium ion intermediate through an electrostatic interaction. Both acids were envisioned to function simultaneously in a "push-pull"-type mechanism. An analogous mechanism has been reported for glycosidases. For example, lysozyme, which cleaves the glycosidic bond of oligosaccharides, has been extensively studied by X-ray crystallography and active-site modeling and predicted to use a carboxylic acid to protonate the exocyclic oxygen of the leaving group and to use another carboxylic acid to stabilize the oxocarbenium ion intermediate (Kirby, 1987). Surprisingly, crystallographic analyses of PNP complexed to sulfate and a variety of pseudosubstrates showed no residues with acidic groups near N7 or the ribosyl oxygen. These results indicated that PNP catalyzes the phosphorolysis of purine nucleosides using a catalytic mechanism substantially different than the glycosidases.

To identify the residues that are important for catalysis, 13 active-site residues were replaced with alanine (Tables 2−4). Results from kinetic studies on each of the mutants indicated that the residues in the ribosyl binding site had little effect on catalysis whereas large decreases in k_{cat} were observed for some residues in the purine and phosphate binding sites. The Asn243Ala mutant exhibited the largest reduction in k_{cat} (1000-fold, Table 2). The magnitude of the reduction was unexpected based on the relatively weak hydrogen bond (>3.2 Å) formed between the carboxamido

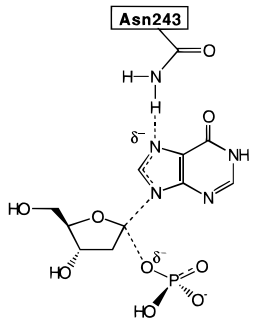

FIGURE 7: Hypothetical TS structure used by PNP.

group of Asn243 and N7 as predicted by both X-ray crystallography and by active-site modeling studies. Since both the glycosidic bond length and N7 negative charge increase during glycosidic bond cleavage, one plausible explanation for the apparent importance of Asn243 in catalysis is that a strong hydrogen bond is formed between Asn243 and N7 in the TS. The increased glycosidic bond length, as predicted from TS modeling of the hydrolytic reaction (Kline & Schramm, 1995), would push the purine base closer to Asn243 whereas the progressive buildup of negative charge on N7 would increase the polarity of the N7−Asn243 interaction and thereby the hydrogen bond strength. Both effects could enhance catalysis since they result in a preferential stabilization of the TS relative to the ground state (Figure 7).

Replacement of either Glu201 or Phe200 with alanine resulted in a large decrease in catalytic efficiency due predominantly to an increase in the K_M for inosine, but also due to an approximate 5−13-fold decrease in k_{cat}. The decrease in k_{cat} is attributed to suboptimal alignment of the purine base for reaction, since it seemed unlikely that either amino acid could preferentially stabilize the TS. The latter explanation was eliminated because glycosidic bond cleavage produces a negatively charged purine base and therefore a TS that is expected to be stabilized by hydrogen bond donation to the negatively charged heteroatoms on the purine ring. Accordingly, a role for Glu201 in TS stabilization appears unlikely, since N1 is an unfavorable site on the purine base to localize electron density originating from the glycosidic bond and since the carboxylate of Glu201 appears to exist as the carboxylic anion and therefore as a hydrogen bond acceptor based on the hydrogen bond pattern observed in the PNP−guanine X-ray structure.

Alanine mutants of ribose binding site residues exhibited k_{cat} values similar to wild-type (Table 3). These results suggested that the hydrogen bonds between Tyr88 and O3′ and between His257 and O5′ are not important for catalysis. Both had previously been speculated to participate in catalysis based on the poor activity of 3′-deoxy purine nucleoside analogs and a TS modeling study which indicated that His257 could participate in TS stabilization through interactions with O5′ (Kline & Schramm, 1993).

In contrast, alanine mutants of phosphate binding site residues exhibited a 5−25-fold decrease in k_{cat} in the phosphorolysis direction and a 50−200-fold decrease in the synthesis direction (Table 4). These results suggest that overall charge and orientation of the phosphate molecule may be important in the TS. Crystallographic studies indicated that the phosphate oxygen poised to add to C1′ of the nucleoside was simultaneously within hydrogen bonding distance of the ϵ2-nitrogen of the His86 imidazole. The

His86 imidazole was also in hydrogen bond contact with the side-chain carboxylate of Glu89 through interaction with the γ1-nitrogen. This structural motif is remarkably similar to the well-studied serine protease catalytic triad (Ser-His-Asp) and therefore suggests that phosphorolysis may require the binding or generation of a phosphate anion with increased negative charge. As in the case of the serine proteases, the Glu−His hydrogen bond may serve to increase the basicity of His86 and therefore to either promote phosphate deprotonation or increase the presence of a positively charged His86 and therefore the selective binding of the phosphate dianion (or trianion). Mutation of His86 and Glu89 to alanine produced mutants with modestly reduced catalytic efficiencies (Table 4). The His86Ala mutant exhibited a 4-fold and 110-fold decrease in k_{cat} in the phosphorolysis and synthetic directions, respectively. The Glu89 mutation had even less of an effect on k_{cat}. The latter result was unexpected based on the complete absence of activity found for the natural PNP mutant, Glu89Lys, which was isolated from a child with a genetic deficiency in PNP (Williams et al., 1987). The difference in activity between the two mutants may arise because of steric constraints or because the lysine side chain presents a positive charge in a location that is constructed to accommodate a negatively charged glutamate. Overall, the results from the alanine mutants suggest that the His86−Glu89 diad is considerably less important for catalysis than the His-Asp portion of the catalytic triad found in serine proteases.

ACKNOWLEDGMENT

We thank Dr. Steve Williams for providing the plasmid containing the hPNP gene and Dr. Per Nygaard (University Institute of Biological Chemistry, Copenhagen, Denmark) for the PNP deficient *E. coli* mutant strain Sϕ312. We also thank Dr. Johanna Stoeckler for critical reading of the manuscript and Ms. Lisa Weston for technical assistance.

REFERENCES

Agarwal, K. C., Agarwal, R. P., Stoeckler, J. D., & Parks, R. E., Jr. (1975) *Biochemistry 14*, 79−84.

Bennett, L. L., Jr., Allan, P. W., Noker, P. E., Rose, L. M., Niwas, S., Montgomery, J. A., & Erion, M. D. (1993) *J. Pharm. Exp. Ther. 266*, 707−714.

Bradford, M. M. (1976) *Anal. Biochem. 72*, 248.

Bzowska, A., Kulikowska, E., & Shugar, D. (1990) *Z. Naturforsh. 45*, 59−70.

Chang, C.-H., Bennett, L. L., Jr., & Brockman, R. W. (1989) *Anal. Biochem. 183*, 279−282.

DeGroot, H., DeGroot, H., & Noll, T. (1985) *Biochem. J. 229*, 255.

Ealick, S. E., Rule, S. A., Carter, D. C., Greenhough, T. J., Babu, Y. S., Cook, W. J., Habash, J., Helliwell, J. R., Stoeckler, J. D., Parks, R. E., Jr., Chen, S.-F., & Bugg, C. E. (1990) *J. Biol. Chem. 265*, 1812−1820.

Ealick, S. E., Babu, Y. S., Bugg, C. E., Erion, M. D., Guida, W. C., Montgomery, J. A., & Secrist, J. A., III (1991) *Proc. Natl. Acad. Sci. U.S.A. 88*, 11540−11544.

Erion, M. D. (1990) *Eur. Patent Appl.* 374,096.

Erion, M. D., Stoeckler, J. D., Guida, W. C., Walter, R. L., & Ealick, S. E. (1997) *Biochemistry 36*, 11735−11748.

Fersht, A. R., Shi, J.-P., Knill-Jones, J., Lowe, D. M., Wilkinson, A. J., Blow, D. M., Brick, P., Carter, P., Waye, M. M. Y., & Winter, G. (1985) *Nature 314*, 235−238.

Friedkin, M. (1950) *J. Biol Chem. 184*, 449−464.

Giblett, E. R., Ammann, A. J., Wara, D. W., Sandman, R., & Diamond, L. K. (1975) *Lancet 1*, 1010−1013.

Goddard, J. M., Caput, D., Williams, S. R., & Martin, D. W., Jr. (1983) *Proc. Natl. Acad. Sci. U.S.A. 80*, 4281−4285.

Jochimsen, B., Nygaard, P., & Veestergaard, T. (1975) *Mol. Gen. Genet. 143*, 85−91.

Jordan, F., & Wu, A. (1978) *J. Med. Chem. 21*, 877−882.

Kalckar, H. M. (1947) *J. Biol. Chem. 167*, 429−443.

Kim, B. K., Cha, S., & Parks, R. E., Jr. (1968) *J. Biol. Chem. 243*, 1771−1776.

Kirby, A. J. (1987) *CRC Crit. Rev. Biochem.* 22, 283−315.

Kline, P. C., & Schramm, V. L. (1992) *Biochemistry 31*, 5964−5973.

Kline, P. C., & Schramm, V. L. (1993) *Biochemistry 32*, 13212−13219.

Kline, P. C., & Schramm, V. L. (1995) *Biochemistry 34*, 1153−1162.

Krenitsky, T. (1967) *Mol. Pharmacol. 3*, 526−536.

Krenitsky, T. A., Koszalka, G. W., & Tuttle, J. V. (1981) *Biochemistry 20*, 3615−3621.

Kunkel, T. A., Roberts, J. D., & Zakour, R. A. (1987) *Methods Enzymol. 154*, 367−382.

Lanzetta, P. A., Alvarez, L., Reinach, P. S., & Candia, O. A. (1979) *Anal. Biochem. 100*, 95−97.

Parks, R. E., Jr., & Agarwal, R. P. (1972) *Enzymes 7*, 3rd ed., 483−514.

Porter, D. J. T. (1992) *J. Biol. Chem. 267*, 7342−7351.

Ropp, P. A., & Traut, T. W. (1991) *J. Biol. Chem. 266*, 7682−7687.

Saheki, S., Takeda, A., & Shimazu, T. (1985) *Anal. Biochem. 148*, 277−281.

Sanger, F., Nicklen, S., & Coulson, A. (1977) *Proc. Natl. Acad. Sci. U.S.A. 74*, 5463.

Sircar, J. C., & Gilbertsen, R. B. (1988) *Drugs of the Future 13*, 653−668.

Stein, R. L., & Cordes, E. H. (1981) *J. Biol. Chem*. 256, 767−772.

Stoeckler, J. D. (1984) in *Developments in Cancer Chemotherapy* (Glazer, R. I., Ed.) pp 35−60, CRC Press: Boca Raton, FL.

Stoeckler, J. D., & Parks, R. E., Jr. (1985) in *Methods in Pharmacology* (Paton, D. M., Ed.) vol 6, pp 147−162, Plenum Press, New York.

Stoeckler, J. D., Cambor, C., & Parks, R. E., Jr. (1980) *Biochemistry 19*, 102−107.

Stoeckler, J. D., Poirot, A. F., Smith, R. M., Parks, R. E., Jr., Ealick, S. E., Takabayashi, K., & Erion, M. D. (1997) *Biochemistry 36*, 11749−11756.

Williams, S. R., Goddard, J. M., & Martin, Jr., D. W. (1984) *Nucleic Acids Res. 12*, 5779−5787.

Williams, S. R., Gekeler, V., McIvor, R. S., & Martin, D. W., Jr. (1987) *J. Biol. Chem. 262*, 2332−2338.

Zimmerman, T. P., Gersten, N. B., Ross, A. F., & Miech, R. P. (1971) *Can. J. Biochem. 49*, 1050−1054.

Zoltewicz, J. A., Clark, D. F., Sharpless, T. W., & Grahe, G. (1970) *J. Am. Chem. Soc. 92*, 1741−1749.

BI961969W